A traveling-wave thermoacoustic cooler designed using particle swarm optimization

Yotaro Kurai, Yuki Ueda

Tokyo University of Agriculture and Technology, Nakacho 2-24-16, Koganei, Tokyo, Japan

Abstract

This study presents the optimization of a traveling-wave thermoacoustic cooler driven by an acoustic driver. The cooler consists of an acoustic driver, a tapered tube, a straight tube, a looped tube, and a regenerator. Its performance critically depends on the characteristics of the straight tube, looped tube, and regenerator. However, the parameters of these components have not previously been optimized simultaneously. In this work, five design parameters were selected for optimization: the lengths of the straight and looped tubes, the length and position of the regenerator, and the radius of the regenerator flow channels. The performance of the cooler was calculated using a coupled numerical model that integrates thermoacoustic theory (including nonlinear acoustic losses) with a damped spring-mass model and an LCR circuit model of the acoustic driver. By combining this comprehensive model with the particle swarm optimization (PSO) method, the five parameters were optimized. A prototype traveling-wave thermoacoustic cooler using atmospheric air as the working gas was then constructed and tested based on the optimized parameters. Experimental results showed that when a $\sqrt{2} \times 15$ V sinusoidal voltage was applied, the acoustic driver consumed 13 W of electrical power (E_{el}) to generate 6 W of acoustic power (W_{in}), producing 7 W of cooling power (Q_C). In comparison, the numerical predictions for E_{el}, W_{in}, and Q_C were 13 W, 6 W, and 11 W, respectively. Although the experimentally obtained cooling power was lower than the numerical prediction, the performance of the prototype exceeded that of previously reported thermoacoustic coolers operating with atmospheric air.

Keywords: Thermoacoustic cooler, Particle Swarm Optimization

1. Introduction

In a thermoacoustic cooler, common gases, such as helium and air, are used as the working medium, and an acoustic wave forces the gas to undergo a thermodynamic cycle. Consequently, a thermoacoustic cooler does not require a refrigerant with high global warming potential and has a simple structure. A thermoacoustic cooler essentially comprises three components. The first is an acoustic driver, which converts electrical power into acoustic power. The second is a tube in which acoustic waves propagate. The third component comprises several narrow flow channels. In this component, the gas interacts thermally with the channel walls and undergoes a thermodynamic cycle. Based on their tube structures, thermoacoustic coolers can be classified into two types: Standing-wave thermoacoustic coolers (SWTCs) and traveling-wave thermoacoustic coolers (TWTCs).

An SWTC has an acoustic driver, a straight tube, and a third component called a stack, which is installed in the straight tube. Owing to the boundary conditions of the straight tube, a standing acoustic wave is excited in the tube. In a standing wave field, the pressure and velocity of a gas parcel oscillate out of phase by ±90 degrees. To generate a thermoacoustic cooling effect, this phase difference requires the condition that the thermal interactions in the stack become irreversible. (Swift (2002); Tominaga (1995); Tijani and J.C.H. Zeegers (2002)) Owing to this irreversibility, the thermodynamic cycle executed in the stack is inherently irreversible. The main design parameters of a SWTC are the flow channel radius, length, and position of the stack. The optimum radius can be theoretically determined (Swift (2002)) and hence, Tijani and Zeegers numerically optimized the length and position of the stack simultaneously.

A TWTC has an acoustic driver, straight tube, looped tube, and a third component called a regenerator. The looped tube is connected to the straight tube, and the regenerator is installed in the looped tube. (Swift et al. (1999); Tijani and Spoelstra (2008)) Because of the structure of the looped tube, the phase difference between the acoustic pressure and velocity oscillations can be zero. (Bassem et al. (2011)) This phase difference allows the gas in the regenerator to undergo a reversible thermodynamic cycle. Therefore, the ideal value of the coefficient of performance (COP) of TWTCs is higher than that of SWTCs. To demonstrate the high potential of a TWTC, Ueda et al. numerically optimized three parameters: the regenerator position in a looped tube, the regenerator length, and the flow channel radius in the regenerator. (Ueda et al. (2010)) They showed that the COP of the TWTC can reach 3.1, corresponding to 60% of the Carnot COP. It should be noted, however, that their analysis assumed an ideal straight tube and an ideal acoustic driver; thus, the effects of the straight-tube parameters and the coupling between the acoustic system and the driver were not considered. Yahya et al. separately optimized the parameters of the tubes,

Email address: uedayuki@cc.tuat.ac.jp (Yuki Ueda)

the regenerator, and the acoustic driver, and demonstrated that the COP, which is defined as the ratio of the cooling power Q_C to acoustic power W_{in} input from the acoustic driver, is approximately 1. (Yahya et al. (2024)) We consider that this value of the COP can be improved by simultaneously optimizing all the parameters. This is because it is known that the value of one parameter can influence the optimal values of the others. (Ueda et al. (2010)) One of the challenges in the simultaneous optimization of a TWTC is that it has a greater number of design parameters compared to a SWTC. This indicates that optimization of design parameters of a TWTC requires the use of an advanced optimization algorithm.

In this study, we propose the use of the particle swarm optimization (PSO) (Kennedy and Eberhart (1995)) to optimize the design parameters of a TWTC. PSO has been applied to various engineering problems (Nasir et al. (2025); Daviran et al. (2025); Bo et al. (2024)) and is suitable for nonlinear systems. Moreover, PSO can be readily coupled with thermoacoustic calculations. (Chaitou and Nika (2012); Rahman and Zhang (2019)) Five design parameters were selected for the optimization: the lengths of the straight and looped tubes, the installation position and length of the regenerator, and the radius of the flow channels within the regenerator. The working gas was atmospheric air and a commercially available loudspeaker was used as an acoustic driver, whose ideal efficiency (Wakeland (2000)) is 0.58. To calculate the performance of the TWTC, a coupled numerical model is used that integrates thermoacoustic theory, accounting for nonlinear acoustic losses, with a damped spring-mass model and an LCR circuit model of the loudspeaker. (Kurai et al. (2025)). The optimization predicted that the COP(= Q_C/W_{in}) reached 2.1 with the loudspeaker's efficiency of 0.50. Based on the optimization results, a TWTC was designed, constructed, and tested. The experimental results showed that when the amplitude of the voltage applied to the acoustic driver was $15\times\sqrt{2}$ V, the electrical input power was 13 W and the input acoustic power was 6.0 W. These values indicate that the efficiency of the driver is 0.46. With the acoustic power, the temperature of the gas at the cold end of the regenerator was reduced to 7.4°C and a cooling power of 6.8 W, which means a COP of 1.1, was obtained. Although the experimentally obtained cooling power was approximately 60% of the numerically predicted value, the performance of the prototype surpassed that of previously reported thermoacoustic coolers operating with atmospheric air. These results demonstrate that PSO is an effective tool for designing TWTCs.

In Sec. 2, the model of a TWTC and its parameters for optimization are described. Section 3 briefly explains the calculation and optimization methods, and Sec. 4 presents the results of the optimization. In Sec. 5, an experimental setup designed based on the optimization is presented and the performance of the setup is demonstrated. The results are summarized in Sec. 6

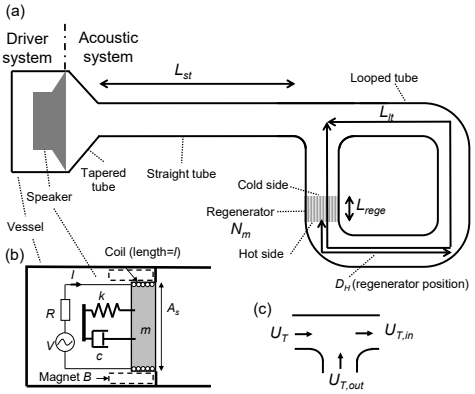

Figure 1: (a) The model of a traveling-wave thermoacoustic cooler, (b) the model of the speaker, and (c) the definitions of the velocities near the T-junction tube.

2. Model

2.1. A Traveling-Wave Thermoacoustic Cooler

The atmospheric air-filled traveling-wave thermoacoustic cooler used for the optimization is illustrated schematically in Fig. 1(a). The cooler can be divided into the driver and acoustic systems. The driver system comprises an acoustic driver and a vessel, whereas the acoustic system comprises a tapered tube, straight tube, T-junction tube, looped tube, and regenerator. There were no hot and cold heat exchangers, and the temperature gradient along the regenerator was not considered in the present calculation. This is because the target cooling temperature in this study was near the ambient temperature and we aimed to reduce the computational costs.

2.2. Driver system

As shown in Fig. 1(b), the acoustic driver was modeled as a spring mass system coupled with an electric circuit through the Lorentz force. The AC voltage applied to the circuit and the corresponding current are denoted as V and I, respectively, and the angular frequency of V and I is defined as ω. As the parameters of the acoustic driver, the experimentally estimated values of the resistance R, self-inductance L_{el}, Bl factor Bl, mass m, spring constant k, and damping coefficient c of the loudspeaker (FW168HS, Fostex ltd.) were used. (Kurai et al. (2024, 2025)) The speaker cone was assumed to be a flat plate and the effective cross-section of the plate A_s was set to 0.014 m^2, as provided by the manufacturer. The value of c was assumed to depend on the displacement magnitude x_s of the flat plate; hence, the driver system exhibited nonlinearity. The volume of the vessel was experimentally estimated, and its effect was included in the spring constant as k_g. Table 1 summarizes the parameters of the speaker located in the vessel, which are the same as those in the previous works (Kurai et al. (2024, 2025)), and are not optimized in this study. The ideal efficiency (Wakeland (2000)) of the speaker is estimated to be 0.58, when $x_s < 2$ mm.

Table 1: The measured parameters of the speaker (FW168HS, Fostex Ltd.) placed in the vessel. (Kurai et al. (2024))

m (g)	24.5
$k + k_g$ (kN/m)	10.6
c (kg/s)	1.1^{*a} $1.1 + 0.085(x_s - 2)^2 + 0.127(x_s - 2)^{*b}$
R (Ω)	6.4
L_{el} (mH)	0.69
Bl (N/A)	9.7

[*a] The value used when $x_s < 2$ mm.
[*b] The equation used when $x_s > 2$ mm.

2.3. Acoustic system

The characteristics of the tapered tube were fixed; specifically, they were not considered as parameters for optimization. The length of the tapered tube was 146 mm. The diameter of the cross-section along the tube changed linearly: The larger end of the tube had a diameter of 145 mm, whereas the smaller end had a diameter of 40 mm. The length L_{st} of the straight tube was set as a parameter for optimization, whereas the diameter was fixed as 40 mm. The T-junction tube was modelled as a point (i.e., it had no length). The looped tube comprised four straight tubes with a diameter of 40 mm and two bent tubes. Total length of the looped tube, L_{lt} was a parameter for optimization; the lengths of the four tubes were set to $L_{lt}/4$, and the lengths of the two bent tubes were set as zero. In the calculation, minor losses were estimated at the tapered tube (Ueda et al. (2020)), T-junction tube (Kurai et al. (2025)), and bent tubes (Kurai et al. (2025)).

The stacked-screen meshes were assumed for the regenerator and the Tanaka-Ueda-Obayashi model (Tanaka et al. (1989); Ueda et al. (2009); Obayashi et al. (2012); Ueda and Farikhah (2016)) was used. In the model, the regenerator is characterized by the effective flow channel radius r_{eff} and the hydraulic diameter d_h. (Ueda et al. (2009)) They can be related to each other through the mesh number N_m and wire diameter d_{wire} of the meshes. The mesh number indicates the number of openings per inch of the mesh sheet. Mesh manufacturers provide tables on the relationship between N_m and d_{wire} and hence, d_{wire} can also be considered a function of N_m. The mesh number N_m and length of the regenerator L_{rege} were selected as optimization parameters. In addition, the distance D_H, which represents the regenerator position as shown in Fig. 1(a), was selected; the subscript H means the hot end of the regenerator. It is known that the closer side of a regenerator to a T-junction becomes its cold side (Ueda et al. (2010); Bassem et al. (2011)), and hence, we set $0 < D_H < L_{lt}/2 - L_{rege} - 0.04$ m. Here, 0.04 m was the minimum value of the distance between the T-junction tube and the cold end of the regenerator of the TWTC constructed in Sec. 5.

3. Calculation method

3.1. Thermoacoustic calculation

As described in Sec. 2.3, five parameters, the straight-tube length L_{st}, looped-tube length L_{lt}, regenerator length L_{rege}, regenerator mesh number N_m, and regenerator position D_H, were used for the optimization. The COP_{total} of the TWTC was set as the objective function for the optimization. It is defined by the cooling power Q_C obtained at the cold end of the regenerator and the electrical power E_{el} required to drive the cooler as

$$\mathrm{COP}_{total} = \frac{Q_C}{E_{el}}. \tag{1}$$

COP_{total} can be also expressed as

$$\mathrm{COP}_{total} = \eta_{speaker} \times \mathrm{COP}, \tag{2}$$

where $\eta_{speaker}$ and COP are defined by acoustic power W_{in} input from the acoustic driver, E_{el}, and Q_C as

$$\eta_{speaker} = \frac{W_{in}}{E_{el}} \tag{3}$$

$$\mathrm{COP} = \frac{Q_C}{W_{in}}, \tag{4}$$

respectively. The reason why we use COP_{total} is that the driver and acoustic systems are affected each other and we wanted to optimize the TWTC with taking into account the driver system efficiency $\eta_{speaker}$, whereas COP(= Q_C/W_{in}) was used in the previous studies(Yahya et al. (2024); Tijani and J.C.H. Zeegers (2002); Ueda et al. (2010); Bassem et al. (2011)).

To calculate Q_C, we employed the thermoacoustic-theory-based method (Kurai et al. (2025)). This method enables the calculation of the transfer matrix (Ueda et al. (2010)) for oscillatory pressure P and velocity U. Here, we define the transfer matrices from the T-junction tube to the cold end of the regenerator as M_C, along the looped tube as M_{loop}, and form the speaker cone to the T-junction tube as M_{tube}. Note that the matrices have nonlinear terms. If the pressure at the T-junction tube, denoted as P_T, is known, it must satisfy the relation

$$\begin{pmatrix} P_T \\ U_{T,out} \end{pmatrix} = M_{loop} \begin{pmatrix} P_T \\ U_{T,in} \end{pmatrix}, \tag{5}$$

where $U_{T,in}$ and $U_{T,out}$ are velocities at the vicinity of the T-junction (see Fig. 1(c)). From this relation, $U_{T,in}$ and $U_{T,out}$ can be obtained. Using P_T, $U_{T,in}$, and M_C, pressure and velocity at the cold end of the regenerator are expressed as

$$\begin{pmatrix} P_C \\ U_C \end{pmatrix} = M_C \begin{pmatrix} P_T \\ U_{T,in} \end{pmatrix}. \tag{6}$$

The acoustic power can then be calculated at the cold end as

$$W_C = \frac{A_C}{2} Re[P_C \tilde{U}_C], \tag{7}$$

where the tilde indicates a conjugate and A_C is the cross-sectional area at the cold end. The value of W_C can be approximated as the cooling power Q_C. This approximation is justified by thermoacoustic theory (Swift (2002); Tominaga (1995)), which states that when the flow channel radius r is much smaller than the thermal penetration depth δ, the absolute value of the acoustic power is equal to that of the cooling power. In a regenerator, r is typically much smaller than δ. Consequently, once P_T is known, Q_C, $U_{T,in}$, and $U_{T,out}$ can be determined.

To calculate E_{el}, a simple electrical circuit equation was coupled with the mass-spring model equation of the speaker cone. The coupled equations can be expressed in matrix form as

$$\begin{pmatrix} P_0 \\ U_0 \end{pmatrix} = M_{speaker} \begin{pmatrix} V \\ I \end{pmatrix} \quad (8)$$

$$M_{speaker} \equiv \begin{pmatrix} -\frac{Z_{mech}}{A_s Bl} & \frac{Z_{\rm mech} Z_{\rm e} + (Bl)^2}{A_s Bl} \\ \frac{1}{Bl}\frac{A_s}{A_0} & -\frac{Z_{\rm e}}{Bl}\frac{A_s}{A_0} \end{pmatrix},$$

where P_0 and U_0 are oscillatory pressure and velocity at the vicinity of the speaker cone, $Z_{\rm mech} \equiv c + i\{\omega m - (k + k_{\rm g})/\omega\}$, $Z_{\rm e} \equiv (R + i\omega L_{el})$, and A_0 is the cross-section of the speaker side of the tapered tube. (Kurai et al. (2024, 2025)) This equation shows that when P_0 and U_0 are known, $M_{speaker}$, which depends on $x_s (= U_0 A_0 / i\omega A s)$ through c, can be calculated, and hence, V and I can be obtained. As a result, E_{el} is determined as

$$E_{el} = \frac{1}{2} Re[V\tilde{I}]. \quad (9)$$

The pressure P_0 and velocity U_0 in Eq. (8) can be related to P_T, $U_{T,out}$, and $U_{T,in}$ as

$$\begin{pmatrix} P'_T \\ U_T \end{pmatrix} = M_{tube} \begin{pmatrix} P_0 \\ U_0 \end{pmatrix} \quad (10)$$

$$P'_T = P_T + \alpha U_T \quad (11)$$

$$U_T = U_{Tin} - U_{T,out} \quad (12)$$

where U_T is the velocity in the connecting point between the straight tube and the T-junction tube (see Fig. 1(c)) and α is a function of $|U_T|$, expressing the effect of the minor loss. (Ueda et al. (2020); Kurai et al. (2025)) Consequently, once P_T is set, (P_0, U_0) is obtained from Eq. (5) and Eqs. (10)-(12), (V, I) is calculated from Eq. (8), and E_{el} is finally evaluated using Eq. (9).

3.2. Optimization method

The PSO method (Kennedy and Eberhart (1995)) was used to optimize the five parameters. As the input conditions, $|V|$ and the frequency of V are set to $15\times\sqrt{2}$ V and 50 Hz, respectively. As described above, the objective function is the COP_{total} and the five parameters are L_{st}, L_{lt}, L_{rege}, N_m, and D_H. The PSO method requires particle numbers i and replication numbers t. Their maximum values were set to $i_{max} = 800$ and $t_{max} = 60$, respectively. The flow chart of the optimization is shown in Fig. 2. The initial values of the five parameters are assigned, and then, a value of P_T that satisfies $|V|/\sqrt{2} = 15$ V is searched. Once such a value of P_T is found, Q_C and E_{el} are evaluated, from which $\mathrm{COP}_{total} (= Q_C / W_{in})$ is calculated. If $t < t_{max}$, the five parameters are updated using the PSO method, whereas if $t = t_{max}$ the calculation is finished.

Here, the method for updating D_H is briefly explained as an example. When $t = t_0 (> 2)$, $\mathrm{COP}_{total,i}(t_0)$ is calculated with $L_{st} = L_{st,i}(t_0)$, $L_{lt,i}(t_0)$, $L_{rege,i}(t_0)$, $N_{m,i}(t_0)$, and $D_{H,i}(t_0)$ using the aforementioned method. Until this step, the number of calculated COP_{total} are $i_{max} \times t_0$. For the next step of t, we update

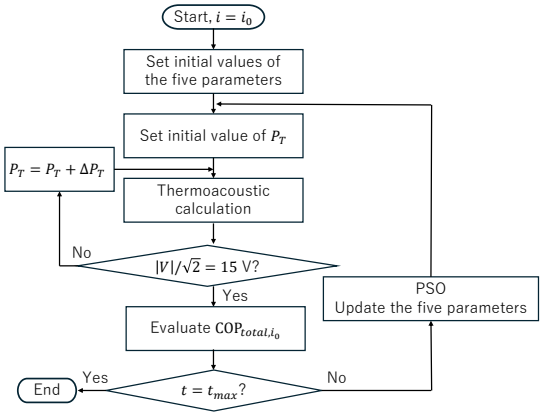

Figure 2: The flow chart of the optimization.

$D_{H,i}(t_0)$ to $D_{H,i}(t_0 + 1)$ using the following equations:

$$\begin{aligned} \delta D_{H,i}(t_0 + 1) &= w\delta D_{H,i}(t_0) \\ &\quad + C_a rand_{a,i}(D_{H,pbest} - D_{H,i}(t_0)) \\ &\quad + C_b rand_{b,i}(D_{H,gbest} - D_{H,i}(t_0)) \quad (13) \\ D_{H,i}(t_0 + 1) &= D_{H,i}(t_0) + \delta D_{H,i}(t_0 + 1). \quad (14) \end{aligned}$$

where w, C_a, and C_b are constant coefficients; $rand_{a,i}$ and $rand_{b,i}$ are random functions ranging from zero to unity; $D_{H,pbest}$ is the best value of D_H found by the particle whose number is i; and $D_{H,gbest}$ is the best value of D_H found by all the particles. With $D_H = D_{H,i}(t_0 + 1)$, $L_{st} = L_{st,i}(t_0 + 1)$, $L_{lt,i}(t_0 + 1)$, $L_{rege,i}(t_0 + 1)$, and $N_{m,i}(t_0 + 1)$, the COP_{total} is re-calculated. When $t = 1$, $D_{H,i}(1)$ is randomly set, $\delta D_{H,i}(1)$ is randomly set to a value between -5 mm to 5 mm, and $D_{H,pbest} = D_{H,i}(1)$. With an increase in t, $\delta D_{H,i}(t)$ is expected to become small and $D_{H,i}(t)$ should saturate, resulting in $D_{H,i}(t) \sim D_{H,pbest} \sim D_{H,gbest}$.

The values of w, C_a, and C_b are tuning parameters in PSO. In this study, these values were determined through iterative testing. The selected values were $w = 0.2$, $C_a = 0.6$, and $C_b = 0.2$ for all five design parameters.

4. Optimization result

Five parameters were simultaneously optimized by the PSO method. In this study, the value of the COP_{total} was calculated 800×60 $(= i_{max} \times t_{max})$ times. For this, our laptop computer required approximately 6 h. In Figs. 3(a)-(e), the five parameters are shown as functions of t, and in Fig. 3(f), the calculated COP_{total}, which is the objective function, is plotted. As can be seen from this figure, all parameters are approximately saturated when t was 60, and a maximum COP_{total} of approximately 0.9 was obtained.

Because the PSO method does not provide a mathematically optimal result, the result generally depends on the calculation conditions such as the initial values of the parameters. Hence, we performed the optimization 28 times. The obtained results about the parameters are summarized in Table 2, in which $\bar{X}$ and σ_X denote the averaged value and the standard derivation of the optimized parameter X, respectively. The data in the table

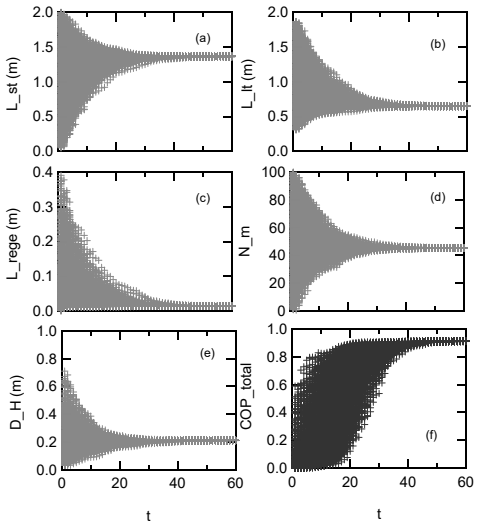

Figure 3: The process of the optimization. (a)-(e) The five parameters are saturated to their optimum values with increasing t and (f) the objective function, namely, COP_{total} reaches the maximum value.

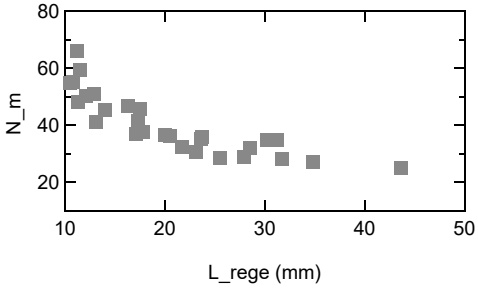

Figure 4: The relationship between the optimized values of L_{rege} and N_m.

show that $\sigma_{L_{rege}}$ and σ_{N_m} are relatively large compared with $\sigma_{L_{st}}$, $\sigma_{L_{lt}}$, and σ_{D_H}. However, it should be noted that $\sigma_{COP_{total}}$ is not large. To elucidate the reason of the large $\sigma_{L_{rege}}$ and σ_{N_m}, the relationship between the optimized L_{rege} and N_m are plotted in Fig. 4, in which 28 points are plotted. This figure implies that the optimum L_{rege} and N_m are not independent of each other. We consider that the important quantity of the regenerator is its flow resistance: when L_{rege} is large, a relatively small value of N_m is favorable, whereas when L_{rege} is small, a large value of N_m is favorable. It was found that a maximum COP_{total} of 1.0 is obtained when L_{rege} = 13 mm and N_m = 41. With these L_{rege} and N_m, $\eta_{speaker}$ becomes 0.50, which is close to the theoretical maximum value 0.58 (Wakeland (2000)) and COP(= W_C/W_{in}) reaches 2.1, which is twice to the previously obtained maximum value (Yahya et al. (2024)).

The total length of the optimum L_{st} and L_{lt} was 2.0 m. Because the frequency was 50 Hz, the ratio of the total length (L_{st} + L_{lt}) and the acoustical wavelength λ was 0.29, which is near 1/4. The ratio of $L_{lt}/(L_{st} + L_{lt})$ was turned out to be important, and the optimum $L_{lt}/(L_{st} + L_{lt})$ was 0.30. It was also found that the optimum D_H/λ was 0.03 and is larger than that of the previous study, in which only two parameters similar to D_H and N_m were optimized. (Ueda et al. (2010)) As previously mentioned, the balance between N_m and L_{rege} is important to be

Table 2: The value of the optimized parameters and experimental values.

parameters	$\bar{X}$	σ_X	ex. value
L_{st} (m)	1.40	0.03	1.32
L_{lt} (m)	0.61	0.04	0.69
L_{rege} (mm)	20	10	15
N_m	40	10	40
D_H(m)	0.21	0.01	0.26
COP_{total}	0.92	0.05	0.89(cal)

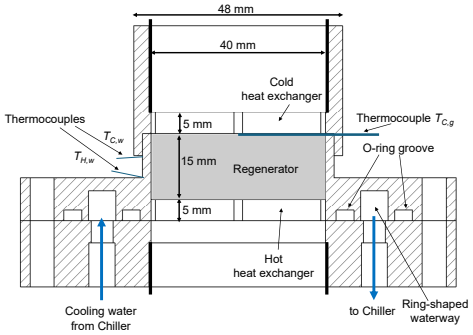

Figure 5: A schematic of the vicinity of the regenerator of the experimental setup.

optimized. If the temperature gradient along the regenerator is large, a long regenerator can be set to prevent a large thermal conduction loss considering the balance.

5. Experiment

5.1. Setup

Based on the optimization result, a TWTC was constructed. The values of the five parameters of the constructed cooler are listed in Table 2. Atmospheric air was used as the working gas. The T-junction and bent tubes were constructed using a 3D printer (F170 Stratasys Ltd.). An AC power supply (EC1000S, NF Corporation) was connected to the speaker to power the cooler. An FFT analyzer (DS5000, Onosokki Ltd.) and voltage and current probes were used to measure V and I. This allowed us to obtain the experimental value of the input electric power $E_{el.ex}$. Pressure sensors were positioned along the straight and looped tubes to measure the oscillatory pressure and velocity (Fusco et al. (1992)). Using the measured pressure and velocity, the acoustic power at the position in the straight tube 0.5-m from the speaker was obtained. This acoustic power is denoted as $W_{in,ex}$. Furthermore, the acoustic power flowing near the cold heat exchanger was estimated from the values of acoustic power measured in the looped and straight tubes. This is denoted as $W_{C,ex}$. We did not measure $W_{C,ex}$ directly because of the short distance between the cold heat exchanger and the T-junction tube; it was not possible to set two pressure sensors along the tube between them.

A schematic of the vicinity of the regenerator is shown in Fig. 5. Hot and cold heat exchangers were installed at the ends of the regenerator. To stop the acoustic mass streaming along

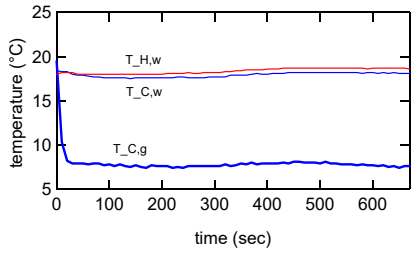

Figure 6: Time dependence of the temperatures $T_{C,g}$, $T_{C,w}$, $T_{H,w}$ with $|V| = 15 \times \sqrt{2}$ V.

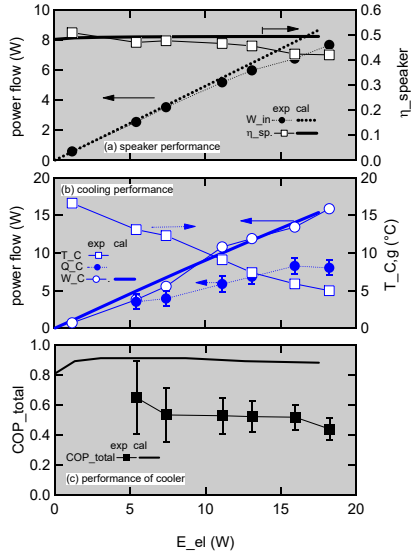

Figure 7: The experimental results of the constructed thermoacoustic cooler. (a) The speaker system performance, (b) cooling power performance, and (c) total performance of the cooler are shown.

the looped tube (Swift et al. (1999)), a membrane was set near the hot heat exchanger. The hot heat exchanger was made of aluminum and was cooled with water whose temperature was approximately 18°C. The regenerator holder and cold heat exchanger were also made of aluminum. The thickness of a part of the wall of the regenerator holder was 2 mm, to which two thermocouples are attached; hence, the heat flow along the holder can be calculated as

$$Q_{C,ex} = \kappa_{AL} \frac{T_{H,w} - T_{C,w}}{\Delta X} (22^2 - 20^2)\pi \times 10^{-6}, \quad (15)$$

where κ_{AL} is the thermal conductivity of aluminum, $T_{H,w}$ and $T_{C,w}$ are the temperatures measured by the thermocouples (Fig. 5), and ΔX is the distance between the temperature measurement points. As the cooling power obtained by the experiment, $Q_{C,ex}$ is used. Another thermocouple was set between the regenerator and cold heat exchanger, and the temperature measured by this thermocouple is denoted as $T_{C,g}$.

5.2. Results

When the magnitude of V was set to $15 \times \sqrt{2}$ V, the experimentally obtained $E_{el,ex}$, $W_{in,ex}$, and $W_{C,ex}$ were 13.1 W, 6.0 W, and 11.7 W, respectively. These values are in good agreement with the calculated results, which are $E_{el} = 12.6$ W, $W_{in} = 6.2$ W, and $W_C = 11.2$ W.

With keeping $|V| = 15 \times \sqrt{2}$ V, the time dependences of temperatures $T_{H,w}$, $T_{C,w}$, and $T_{C,g}$ were measured and are plotted in Fig. 6. As can be seen from this figure, the temperature $T_{C,g}$ was rapidly reduced, and reached 10.3°C when the experimental time was 10 s. Then, $T_{C,g}$ gradually decreased to 7.6°C. Due to the action of the cooling water, the initial $T_{H,w}$ and $T_{C,w}$ were lower than $T_{C,g}$, and $T_{H,w}$ and $T_{C,w}$ slowly decreased and slightly fluctuated. The temperature difference $(T_{H,w} - T_{C,w})$ became approximately constant at 0.5°C after 220 s, leading to $Q_{C,ex} = 6.8 \pm 0.8$ W. Therefore, the COP_{total} of the constructed TWTC was 0.52. The value of $Q_{C,ex}$ was approximately 60% of $W_{C,ex}$, although W_C was assumed to be equal to Q_C in the calculation. One of the reasons for the relatively large difference between $Q_{C,ex}$ and $W_{C,ex}$ is the experimental setup used. As shown in Fig. 5, the wall thickness of the tube with the cold heat exchanger was 4 mm; thus the cooling power was lost from the cold heat exchanger to the upper side in Fig. 5 owing to the thermal conduction along the tube wall.

The abovementioned performance measurements were performed by changing E_{el}. Figure 7(a) shows the measured performance of the speaker as a function of the input power E_{el}. As shown in Fig. 7(a), the input acoustic power $W_{in,ex}$ agrees well with the calculated result, and the experimentally obtained efficiency $\eta_{speaker,ex} = W_{in,ex}/E_{el,exp}$ was within 0.46 ± 0.04. This value is approximately 80% of the ideal efficiency (Wakeland (2000)) of the used loudspeaker, which is 0.58. Therefore, we believe that acoustic matching between the acoustic and driver systems was achieved in this optimized experimental setup.

In Fig. 7(b), $Q_{C,ex}$, $W_{C,ex}$, and $T_{C,g}$ are plotted as functions of E_{el} by symbols. The temperature $T_{C,g}$ decreased with increasing in $E_{el,exp}$, and when $E_{el,exp} = 18.2$ W, the lowest temperature of $T_{C,g} = 5.0$°C was obtained. The value of $W_{C,ex}$ matches the calculated W_C shown by the solid line. However, $W_{C,ex}$ does not agree with $Q_{C,ex}$, when $E_{el,exp}$ is large. This resulted in the disagreement between the calculated and measured COP_{total}, as shown in Fig. 7(c). As mentioned above, the disagreement between $W_{C,ex}$ and $Q_{C,ex}$ was attributed to the problem of the constructed experimental setup. The highest $Q_{C,exp}$ (=8.3 W) was obtained with $\mathrm{COP}_{total} = 0.52$ when $E_{el,exp} = 16$ W. These values of $Q_{C,exp}$ and COP_{total} are higher than those of previously constructed atmospheric-air-filled thermoacoustic coolers(Shimokawa et al. (2009); Poese (2004)).

6. Summary

A traveling-wave thermoacoustic cooler (TWTC) was optimized by coupling a thermoacoustic-theory-based calculation with the particle swarm optimization (PSO) method. In the thermoacoustic-theory-based calculation, nonlinear losses known as acoustic minor losses, a physical model of the acoustic driver, and an electrical circuit model of the acoustic driver were incorporated. In the PSO method, the total coefficient of performance (COP_{total}), defined as the ratio of cooling power Q_C to input electric power E_{el}, was set as the objective function, and five key design parameters of the TWTC were considered.

The optimization showed that COP_{total} = 1.0 can be achieved with a speaker efficiency of $\eta_{speaker}$ = 0.50. This COP_{total} is higher than those reported in previous studies, and the $\eta_{speaker}$ value is close to its theoretical upper limit.

Based on the optimized design, a TWTC was constructed and tested. The experimentally obtained Q_C, $\eta_{speaker}$, and COP_{total} were 6.8 W, 0.46, and 0.52, respectively, compared with the numerically predicted values of 11 W, 0.49, and 0.89. Although the experimental cooling power and total COP were lower than the numerical predictions, the prototype outperformed previously reported thermoacoustic coolers operating with atmospheric air. These results demonstrate that combining thermoacoustic-theory-based calculations with the PSO method is an effective approach for designing a TWTC.

Acknowledgments

This work was supported by JSPS KAKENHI Grant Number 22H01966.

During the preparation of this work the authors used ChatGPT in order to improve the English quality. After using this tool, the authors reviewed and edited the content as needed and take full responsibility for the content of the publication.

References

G. W. Swift, Thermoacoustics: A Unifying Perspective for Some Engines and Refrigerators, Acoustical Society of America, Pennsylvania, 2002.

A. Tominaga, Thermodynamic aspect of thermoacoustic phenomena, Cryogenics 35 (1995) 427–440.

M. Tijani, A. d. W. J.C.H. Zeegers, Design of thermoacoustic refrigerators, Cryogenics 42 (2002) 49–57.

G. W. Swift, D. L. Gardner, S. Backhaus, Acoustic recovery of lost power in pulse tube refrigerators, J. Acoust. Soc. Am. 105 (1999) 711–724.

M. Tijani, S. Spoelstra, Study of a coaxial thermoacoustic-stirling cooler, Cryogenics 48 (2008) 77–82.

M. M. Bassem, Y. Ueda, A. Akisawa, Thermoacoustic stirling heat pump working as a heater, Applied Physics Express 4 (2011) 107301.

Y. Ueda, M. M. Bassem, K. Tsuji, A. Akisawa, Optimization of the regenerator of a traveling-wave thermoacoustic refrigerator, J. Appl. Phys. 107 (2010) 034901.

S. G. Yahya, A. Hamood, A. J. Jaworski, X. Mao, Development of a two-stage thermoacoustic refrigerator prototype, International Journal of Thermofluids 24 (2024) 100903.

J. Kennedy, R. Eberhart, Particle swarm optimization, in: Proceedings of ICNN'95 - International Conference on Neural Networks, volume 4, 1995, pp. 1942–1948 vol.4.

N. M. Nasir, N. M. A. Ghani, A. N. K. Nasir, M. A. Ahmad, M. O. Tokhi, Neuro-modelling and fuzzy logic control of a two-wheeled wheelchair system, Journal of Low Frequency Noise, Vibration and Active Control 44 (2025) 588–602.

M. Daviran, A. Maghsoudi, R. Ghezelbash, Optimized ai-mpm: Application of pso for tuning the hyperparameters of svm and rf algorithms, Computers & Geosciences 195 (2025) 105785.

Y. Bo, X. Guo, Q. Liu, Y. Pan, L. Zhang, Y. Lu, Prediction of tunnel deformation using pso variant integrated with xgboost and its tbm jamming application, Tunnelling and Underground Space Technology 150 (2024) 105842.

H. Chaitou, P. Nika, Exergetic optimization of a thermoacoustic engine using the particle swarm optimization method, Energy Conversion and Management 55 (2012) 71–80.

A. A. Rahman, X. Zhang, Single-objective optimization for stack unit of standing wave thermoacoustic refrigerator through particle swarm optimization method, Energy Procedia 158 (2019) 5445–5452. innovative Solutions for Energy Transitions.

R. S. Wakeland, Use of electrodynamic drivers in thermoacoustic refrigerators, The Journal of the Acoustical Society of America 107 (2000) 827–832.

Y. Kurai, S. Sekimoto, Y. Ueda, Modeling of components of a traveling-wave thermoacoustic refrigerator taking into account nonlinear losses, Acoustical Science and Technology 46 (2025) 286–294.

Y. Kurai, S. Sekimoto, Y. Ueda, Measurement of characteristics of loudspeaker required for combination with thermoacoustic devices, The Journal of the Acoustical Society of Japan 80 (2024) 367–373.

Y. Ueda, S. Yonemitsu, K. Ohashi, T. Okamoto, Measurement and empirical evaluation of acoustic loss in tube with abrupt area change, The Journal of the Acoustical Society of America 147 (2020) 364–370.

M. Tanaka, I. Yamashita, F. Chisaka, Flow and heat transfer characteristics of stirling engine regenerator in oscillating flow, Transactions of the JSME (in Japanese) 55 (1989) 2478–2485.

Y. Ueda, T. Kato, C. Kato, Experimental evaluation of the acoustical properties of stacked-screen regenerators, J. Acoust. Soc. Am. 125 (2009) 780–786.

A. Obayashi, S.-H. Hsu, T. Biwa, Amplitude dependence of thermoacoustic properties of stacked wire meshes, TEION KOGAKU (Journal of Cryogenics and Superconductivity Society of Japan) 47 (2012) 562–567.

Y. Ueda, I. Farikhah, Calculation of the energy conversion efficiency of a stacked-screen regenerator using thermoacoustic theory, TEION KOGAKU (Journal of Cryogenics and Superconductivity Society of Japan) 51 (2016) 403–408.

M. Bassem, Y. Ueda, A. Akisawa, Design and construction of a traveling-wave thermoacoustic refrigerator, Int. J. Refrigeration 34 (2011) 1125–1131.

A. M. Fusco, W. C. Ward, G. W. Swift, Two-sensor power measurements in lossy ducts, J. Acoust. Soc. Am. 91 (1992) 2229–2235.

S. Shimokawa, Y. Ueda, A. Akisawa, Experimental design optimization of a traveling-wave thermoacoustic refrigerator filled with atmospheric air(thermal engineering), Transactions of the Japan Society of Mechanical Engineers Series B 75 (2009) 1351–1356.

M. E. Poese, An Evolution of Compact Thermoacoustic Refrigerator Design, Ph.D. thesis, The Pennsylvania State University, 2004.